Inorg. Chem. **2008**, *47*, 7523−7534

Syntheses, Structures, and Spectroscopic Properties of $K_9Nd[PS_4]_4$, $K_3Nd[PS_4]_2$, $Cs_3Nd[PS_4]_2$, and $K_3Nd_3[PS_4]_4$

Yuandong Wu and Wolfgang Bensch*

Institut für Anorganische Chemie, Universität Kiel, Olshausenstr. 40, D24098 Germany

Received January 24, 2008

Four new quaternary alkali neodymium thiophosphates $K_9Nd[PS_4]_4$ (**1**), $K_3Nd[PS_4]_2$ (**2**), $Cs_3Nd[PS_4]_2$ (**3**), and $K_3Nd_3[PS_4]_4$ (**4**) were synthesized by reacting Nd with in situ formed fluxes of K_2S_3 or Cs_2S_3, P_2S_5 and S in appropriate molar ratios at 973 K. Their crystal structures are determined by single crystal X-ray diffraction. Crystal data: **1:** space group *C*2/*c*, $a = 20.1894(16)$, $b = 9.7679(5)$, $c = 17.4930(15)$ Å, $\beta = 115.66(1)°$, and $Z = 4$; **2:** space group $P2_1/c$, $a = 9.1799(7)$, $b = 16.8797(12)$, $c = 9.4828(7)$ Å, $\beta = 90.20(1)°$, and $Z = 4$; **3:** space group $P2_1/n$, $a = 15.3641(13)$, $b = 6.8865(4)$, $c = 15.3902(13)$ Å, $\beta = 99.19(1)°$, and $Z = 4$; **4:** space group *C*2/*c*, $a = 16.1496(14)$, $b = 11.6357(7)$, $c = 14.6784(11)$ Å, $\beta = 90.40(1)°$, and $Z = 4$. The structure of **1** is composed of one-dimensional $^1_\infty\{Nd[PS_4]_4\}^{9-}$ chains and charge balancing K^+ ions. Within the chains, eight-coordinated Nd^{3+} ions, which are mixed with K^+ ions, are connected by $[PS_4]^{3-}$ tetrahedra. The crystal structures of **2** and **3** are characterized by anionic chains $^1_\infty\{Nd[PS_4]_2\}^{3-}$ being separated by K^+ or Cs^+ ions. Along each chain the Nd^{3+} ions are bridged by $[PS_4]^{3-}$ anions. The difference between the structures of **2** and **3** is that in **2** the Nd^{3+} ions are coordinated by four edge-sharing $[PS_4]^{3-}$ tetrahedra while in **3** each Nd^{3+} ion is surrounded by one corner-sharing, one face-sharing, and two edge-sharing $[PS_4]^{3-}$ tetrahedra. The structure of **4** is a three-dimensional network with K^+ cations residing in tunnels running along [110] and [$\bar{1}$10]. The {Nd(1)S_8} polyhedra share common edges with four $[PS_4]$ tetrahedra forming one-dimensional chains $^1_\infty\{Nd[PS_4]_2\}^{3-}$ running along [110] and [$\bar{1}$10]. The chains are linked by {Nd(2)S_8} polyhedra yielding the final three-dimensional network $^3_\infty\{Nd[PS_4]_2\}^{3-}$. The internal vibrations of both crystallographically independent $[PS_4]^{3-}$ anions of **2**−**4** have been assigned in the range 200−650 cm^{-1} by comparison of their corresponding far/mid infrared and Raman spectra ($\lambda_{exc} = 488$ nm) on account of locally imposed C_1 symmetry. In the Fourier-transform-Raman spectrum ($\lambda_{exc} = 1064$ nm) of **2**−**4**, very similar well-resolved electronic Raman (ER) transitions from the electronic Nd^{3+} ground-state to two levels of the $^4I_{9/2}$ ground manifold and to the six levels of the $^4I_{11/2}$ manifold have been determined. Resonant Raman excitation via a B-term mechanism involving the $^4I_{15/2}$ and $^4F_{3/2}$ intermediate states may account for the significant intensity enhancement of the ER transitions with respect to the symmetric P−S stretching vibration ν_1. Broad absorptions in the UV/vis/NIR diffuse reflectance spectrum at 293 K in the range 5000−25000 cm^{-1} of **2**−**4** are attributed to spin-allowed excited quartet states [^{4}(I < *F* < S < G < D)] and spin-forbidden doublet states [^{2}(H < G < K < D < P)] of Nd^{3+}. A luminescense spectrum of **3** obtained at 15 K by excitation with 454.5 nm shows multiplets of narrow lines that reproduce the Nd^{3+} absorptions. Sharp and intense luminescence lines are produced instead by excitation with 514.5 nm. Lines at 18681 ($^4G_{7/2}$), 16692 ($^4G_{5/2}$), 14489 ($^4F_{9/2}$), and 13186 cm^{-1} ($^4F_{7/2}$) coincide with the corresponding absorptions. Hypersensitive $^4G_{5/2}$ is split by 42 cm^{-1}. The most intense multiplet at about 16500 cm^{-1} is assigned to the transition from $^4G_{5/2}$ to the Stark levels of the ground manifold $^4I_{9/2}$.

1. Introduction

Since the structural characterization of the first rare earth thiophosphate $Eu_2[P_2S_6]$[1] and the discovery of the luminescent properties of the $Ln[PS_4]$ family,[2] the explorative investigation of rare earth chalcophosphates increased significantly and a fascinating variety of new quaternary compounds with structures ranging from separated ions to three-dimensional networks were reported. Examples are $TlEu[PS_4]$,[3] $KLa[P_2Se_6]$,[4] $K_4Eu[PSe_4]_2$,[5] $KLn[P_2Se_6]$

* To whom correspondence should be addressed. E-mail: wbensch@ac.uni-kiel.de. Fax: +49-431-8801520.

(1) Brockner, W.; Becker, R. *Z. Naturforsch.* **1987**, *42a*, 511–512.

10.1021/ic800143x CCC: $40.75
Published on Web 08/08/2008

(Ln = Y, La, Ce, Pr, Gd),[6] $Rb_9Ce[PSe_4]_4$,[7] $A_3Ln[P_2Se_8]$, $A_2Ln[P_2Se_7]$ (A = Rb, Cs; Ln = Ce, Gd),[8] $K_3Ce[P_2S_8]$,[9] $K_9Ce[P_4S_{16}]$,[10] $LiEu[PSe_4]$, $KEu[PSe_4]$,[11] $K_2La[P_2Q_7]$, $K_3La[PQ_4]_2$, $K_6La[PQ_4]_3$, $K_{9-x}La_{1+x/3}[PQ_4]_4$ ($x = 0.5$), $KEu[PQ_4]$ (Q = S, Se), $KLa[P_2S_6]$, $K_4Eu[P_2S_6]$,[12] $NaYb[P_2S_6]$,$NaSm[P_2S_6]$,$KSm[P_2S_7]$,[13]and$NaCe[P_2Se_6]$,$Cu_{0.4}Ce_{1.2}[P_2Se_6]$, $Ce_4[P_2Se_6]_3$, $AgCe[P_2Se_6]$,[14] $K_2Nd[P_2S_7]$,[15] $K_3Ce_2[P_3S_{12}]$,[16] $Rb_3Ln_3[PS_4]_4$ (Ln = Pr, Er),[17] $K_6Yb_3[PS_4]_5$,[18] $LiEu[PS_4]$,[2i] $Cs_3Pr_5[PS_4]_6$,[19] $Cs_4Pr_2[PS_4]_2[P_2S_6]$,[20] $Li_9Gd_2[PS_4]_5$,[21] $Tl_2CeP_2S_7$,[22] $AgScP_2S_6$,[23] and $Ba_3Ln_2[P_4S_{16}]$.[24] Most of these compounds contain potassium and were synthesized in chalcogenophosphate fluxes. In our continuing explorative work we focused our attention on the A−Nd−P−S system because only few Nd based thiophosphates have been reported until now. Furthermore, we are interested to recognize the effect of the radius of the alkali cation on the structures of rare earth thiophosphates when applying identical reaction conditions.

In this contribution we report the syntheses and crystal structures of the new quaternary thiophosphates $K_9Nd[PS_4]_4$ (**1**), $K_3Nd[PS_4]_2$ (**2**), $Cs_3Nd[PS_4]_2$ (**3**), and $K_3Nd_3[PS_4]_4$ (**4**) for which one-dimensional and three-dimensional anionic structures are observed. The results demonstrate the remarkable diversity of rare earth containing chalcophosphate compounds.

2. Experimental Section

2.1. Reagents. The following reagents were used as obtained unless especially noted: (i) K and Cs metal, 99.0%, ABCR GmbH & Co.KG; (ii) P_2S_5, 99.99%, Alfa Aesar; (iii) Nd powder, 99.99%, 200 mesh, Alfa Aesar; (iv) As_2S_3 powder, 99.9%, ABCR GmbH & Co.KG; (v) S powder, 99.99%, Heraeus; (vi) BaS powder, 99.99%, Alfa Aesar.

2.2. Syntheses. General: K_2S_3 and Cs_2S_3 were prepared from the reaction of stoichiometric amounts of elemental K or Cs and S powder in liquid ammonia under an argon atmosphere. For all syntheses the starting materials were first thoroughly mixed and loaded into fused silica ampoules in a nitrogen filled glovebox. Afterward the ampoules were sealed under vacuum to 2×10^{-3} mbar. The heating treatments were done in computer-controlled furnaces.

Preparation of $K_9Nd[PS_4]_4$ (1). The ampoule containing the starting materials of K_2S_3, Nd, P_2S_5, S in a molar ratio of 2:1:0.5:6 was heated to 973 K and remained at this temperature for 5 days. The furnace was then allowed to cool down to 373 K at a rate of 3 K/h followed by cooling to room temperature in 4 h. Crystals were separated from excess flux by washing the reaction products with dimethylformamide (DMF) and acetone. The product consisting of transparent pale red crystals (yield: 10% based on Nd) was dried in vacuum. An energy dispersive X-ray spectroscopy (EDX) analysis of single crystals indicated the presence of all four elements (K, Nd, P, S) in an approximately ratio of 9:1:4:16.

Preparation of $K_3Nd[PS_4]_2$ (2). A mixture of K_2S_3, BaS, Nd, P_2S_5, and S powders in a molar ratio of 2:0.25:1:1:6 was heated to 973 at 30 K/h, kept at 973 K for 5 days, cooled at 3 K/h to 373 K, and then the furnace was turned off. The excess flux was removed from the reaction mixture by washing with DMF, followed by drying with acetone. The reaction product consisted of transparent colorless platelet crystals (~70% yield) which were stable in air and moisture. The EDX analysis of several crystals indicated the only presence of four elements (K, Nd, P, S) in an approximately ratio of 3:1:2:8. In further experiments compound **2** was synthesized applying K_2S_3, Nd, P_2S_5, S in a molar ratio of 2:1:1:6. The reaction product was treated in the same way described above and contained **2** in about 90% yield.

Preparation of $Cs_3Nd[PS_4]_2$ (3). 3 was synthesized applying the procedure for **2** except that Cs_2S_3, Nd, P_2S_5, As_2S_3, and S were used as starting materials in a ratio of 2:1:1:0.5:6. The reaction product consisted of transparent colorless polyhedral crystals (~70% yield) which were stable to air and moisture. The EDX analysis revealed the presence of Cs, Nd, P, and S in an approximately ratio of 3:1:2:8. Compound **3** could also be prepared from reacting the mixture Cs_2S_3, Nd, P_2S_5, S in a molar ratio of 2:1:1:6. After treatment of the reaction product (see above), **3** was obtained in about 90% yield.

Preparation of $K_3Nd_3[PS_4]_4$ (4). The procedure for the synthesis of **4** is the same as that of **1** except that the molar ratio of K_2S_3,

(2) (a) Komm, T.; Gudat, D.; Schleid, T. *Z. Naturforsch.* **2006**, *61b*, 766–774. (b) Gauthier, G.; Jobic, S.; Boucher, F.; Macaudière, P.; Huguenin, D.; Rouxel, J.; Brec, R. *Chem. Mater.* **1998**, *10*, 2341–2347. (c) Wibbelmann, C.; Brockner, W.; Eisenmann, B.; Schäfer, H. *Z. Naturforsch.* **1984**, *39a*, 190–194. (d) Huang, Z.-L.; Cajipe, V.; Molinie, P. *J. Rare Earths* **1998**, *16*, 167–171. (e) Huang, Z.-L.; Cajipe, V.; Molinie, P. *J. Rare Earths* **1999**, *16*, 6–11. (f) Voloniva, A. N.; Koubchinova, T. B.; Maximova, S. I.; Murav′ev, E. N.; Niyazov, S. A.; Orlovskii, V. P.; Palkina, K. K.; Chibikova, N. T. *Zh. Noorg. Khim.* **1987**, *32*, 2899–2901. (g) Palkina, K. K.; Maksimova, S. I.; Chibiskova, N. T.; Kuvshinova, T. B.; Volodina, A. N. *Neorg. Mater.* **1984**, *20*, 1557–1560. (h) LeBret, G. C.; McCoy, H. C.; Kittelstved, K. R.; Cleary, D. A.; Twamley, B. *Inorg. Chim. Acta* **2003**, *343*, 141–146. (i) Jörgens, S.; Alili, L.; Mewis, A. *Z. Naturforsch.* **2005**, *60b*, 705–708. (j) Palkina, K. K.; Kuvshinova, T. B.; Maksimova, S. I.; Chibiskova, N. T.; Tripol'skaya, T. A. *Neorg. Mater.* **1989**, *25*, 1555–1556. (k) Le Rolland, B.; McMillan, P.; Molinie, P.; Colombet, P. *Eur. J. Solid State Inorg. Chem.* **1990**, *27*, 715–724.

(3) Carillo-Cabrera, W.; Peters, K.; von Schnering, H. G. *Z. Anorg. Allg. Chem.* **1995**, *621*, 557–561.

(4) Chen, J. H.; Dorhout, P. K. *Inorg. Chem.* **1995**, *34*, 5705–5706.

(5) Chondroudis, K.; McCarthy, T. J.; Kanatzidis, M. G. *Inorg. Chem.* **1996**, *35*, 840–844.

(6) Chen, J. H.; Dorhout, P. K.; Ostenson, J. E. *Inorg. Chem.* **1996**, *35*, 5627–5633.

(7) Chondroudis, K.; Kanatzidis, M. G. *Inorg. Chem. Commun.* **1998**, *1*, 55–57.

(8) Chondroudis, K.; Kanatzidis, M. G. *Inorg. Chem.* **1998**, *37*, 3792–3797.

(9) Gauthier, G.; Jobic, S.; Brec, R.; Rouxel, J. *Inorg. Chem.* **1998**, *37*, 2332–2333.

(10) Gauthier, G.; Jobic, S.; Danaire, V.; Brec, R.; Evain, M. *Acta Crystallogr.* **2000**, *C56*, e117.

(11) Aitken, J. A.; Chondroudis, K.; Young, V. G., Jr.; Kanatzidis, M. G. *Inorg. Chem.* **2000**, *39*, 1525–1533.

(12) (a) Evenson, C. R., IV; Dorhout, P. K. *Inorg. Chem.* **2001**, *40*, 2884–2891. (b) Evenson, C. R., IV; Dorhout, P. K. *Inorg. Chem.* **2001**, *40*, 2875–2883.

(13) Goh, E.-Y.; Kim, E.-J.; Kim, S.-J. *J. Solid State Chem.* **2001**, *160*, 195–204.

(14) Aitken, J. A.; Evain, M.; Iordanidis, L.; Kanatzidis, M. G. *Inorg. Chem.* **2002**, *41*, 180–191.

(15) Schleid, T.; Hartenbach, I.; Komm, T. *Z. Anorg. Allg. Chem.* **2002**, *628*, 7–9.

(16) Gauthier, G.; Evain, M.; Jobic, S.; Brec, R. *Solid State Sci.* **2002**, *4*, 1361–1366.

(17) Komm, T.; Schleid, T. *J. Solid State Chem.* **2005**, *178*, 454–463.

(18) Aitken, J. A.; Kanatzidis, M. G. *J. Am. Chem. Soc.* **2004**, *126*, 11780–11781.

(19) Komm, T.; Schleid, T. *Z. Anorg. Allg. Chem.* **2004**, *630*, 712–716.

(20) Komm, T.; Schleid, T. *Z. Kristallogr. Suppl.* **2003**, *20*, 152.

(21) Komm, T.; Schleid, T. *J. Alloys Compd.* **2006**, *418*, 106–110.

(22) McGuire, M. A.; Reynolds, T. K.; DiSalvo, F. J. *Chem. Mater.* **2005**, *17*, 2875–2884.

(23) Lee, S.; Colombet, P.; Ouvrard, G.; Brec, R. *Inorg. Chem.* **1988**, *27*, 1291–1294.

(24) Klawitter, Y.; Bensch, W.; Wickledder, C. *Chem. Mater.* **2006**, *18*, 187–197.

Table 1. Technical Details of Data Acquisition and Some Refinement Results[a]

compound	**1**	**2**	**3**	**4**
formula	$K_9Nd[PS_4]_4$	$K_3Nd[PS_4]_2$	$Cs_3Nd[PS_4]_2$	$K_3Nd_3[PS_4]_4$
crystal system	monoclinic	monoclinic	monoclinic	monoclinic
space group	*C2/c*	$P2_1/c$	$P2_1/n$	*C2/c*
a [Å]	20.1894(16)	9.1799(7)	15.3641(13)	16.1496(14)
b [Å]	9.7679(5)	16.8797(12)	6.8865(4)	11.6357(7)
c [Å]	17.4930(15)	9.4828(7)	15.3902(13)	14.6784(11)
β [°]	115.66(1)	90.20(1)	99.19(1)	90.40(1)
V [Å^3]	3109.5(4)	1469.4(2)	1607.5(2)	2758.2(4)
Z	4	4	4	4
T [K]	220	220	220	220
calcd. den. (g.cm^{-3})	2.440	2.622	3.559	2.858
μ Mo [mm^{-1}]	4.286	5.697	11.127	7.454
F(000)	2202	1100	1532	2212
2θ range [°]	$5° \le 2\theta \le 56°$	$5° \le 2\theta \le 56°$	$5° \le 2\theta \le 56°$	$5° \le 2\theta \le 56°$
index range	$-26 \le h \le 25$	$-12 \le h \le 12$	$-20 \le h \le 20$	$-19 \le h \le 21$
	$-12 \le k \le 12$	$-22 \le k \le 22$	$-9 \le k \le 9$	$-14 \le k \le 15$
	$-23 \le l \le 23$	$-12 \le l \le 12$	$-20 \le l \le 19$	$-19 \le l \le 19$
indep. refl.	3729	3431	3857	3238
refl. [$F_o > 4\sigma(F_o)$]	2595	3251	3131	2894
R_{int}	0.0305	0.0611	0.0494	0.0381
min/max. transm.	0.4457/0.6170	0.3073/0.5195	0.1513/0.3293	0.3028/0.3979
no. parameters	140	129	128	121
*a**	0.0583	0.0680	0.0609	0.0596
*b**	8.8	4.9	0	0
*R*1 for $Fo > 4\sigma(Fo)$	0.0361	0.0393	0.0343	0.0302
*wR*2 for all data	0.1104	0.1061	0.0911	0.0792
GOF	1.081	1.073	0.993	0.993
$\Delta\rho$[e Å^{-3}]	1.218/−1.256	3.475/−2.043	1.653/−2.150	1.677/−2.511

[a] $R1 = \sum||F_o| - |F_c||/\sum|F_o|$, $wR2 = [\sum(F_o^2 - F_c^2)^2/\sum w(F_o^2)^2]^{1/2}$, $w = 1/[\sigma(F_o^2) + (aP)^2 + bP]$ where $P = (\max(F_o^2,0) + 2F_c^2)/3$.

BaS, Nd, P_2S_5, and S was changed to 1:1:1:6. The melt contained transparent platelet crystals in 90% yield. The crystals were stable in dry air for several weeks. The EDX analysis indicated the presence of K, Nd, P, and S in the approximate ratio of 3:3:4:16.

2.3. Physical Measurements. X-ray Crystallography. All single crystal X-ray investigations were performed using an Imaging Plate Diffraction System (IPDS-1; Mo Kα-radiation; $\lambda = 0.71073$ Å) equipped with a low temperature device from Oxford Cryosystem. The crystals were mounted on top of glass fibers and bathed in cold nitrogen stream during data collection. The raw intensities were treated in the normal way by Lorentz, polarization, and numerical absorption corrections. All structures were solved with direct methods using SHELXS-97 and refined against F_o^2 using SHELXL-97 of the SHELXTL program package.[25]

$K_9Nd[PS_4]_4$ (1). A transparent pale red platelet crystal with dimensions of 0.13 × 0.10 × 0.08 mm^3 was manually selected from the reaction product. From systematic extinctions, the space group *C*2/*c* was chosen. The structure refinement revealed unusually anisotropic displacement parameters for the Nd atoms. Almost all P and S sites showed non-positive principal mean square atomic displacements. Introducing a disorder model with mixed Nd/K occupancies on the Nd sites, the refinement resulted in 35.2% K on the Nd(1) site and 56.1% K on the Nd(2) position. The final refined composition was $K_{8.91(1)}Nd_{1.09(1)}[PS_4]_4$. In contrast to $K_9Ce[PS_4]_4$,[10] no evidence of merohedrally twinning was found. The refinement was also carried out in the space group *C*2 with twinning by an inversion center (Flack parameter $x = 0.0(8)$). But no essential differences of the final structural features were found, especially the Nd/K disorder was not removed in the non-centrosymmetric space group.

$K_3Nd[PS_4]_2$ (2). A transparent colorless platelet crystal with dimensions of 0.14 × 0.09 × 0.07 mm^3 was manually selected from the reaction product. Space group $P2_1/c$ was chosen on the basis of the systematic absences. At the early stages of the refinement the reliability factors R1 and wR2 were 0.15 and 0.42. To improve the refinement the TwinRotMat option in PLATON[26] was used to determine the twin law for the crystal (−1 0 0, 0 1 0, 0 0 1) or (1 0 0, 0 −1 0, 0 0 −1). A separate set of batch scale factors was refined. With this strategy the reliability factors were significantly improved. In the final stage all atoms were refined with anisotropic displacement parameters yielding R1 = 0.0393 and wR2 = 0.1061. The maximum and minimum peaks in the final Fourier difference map were 3.475 and −2.043 e/Å^3.

$Cs_3Nd[PS_4]_2$ (3) and $K_3Nd_3[PS_4]_4$ (4). A transparent colorless platelet crystal with dimensions of 0.15 × 0.10 × 0.06 mm^3 for **3** and a transparent colorless polyhedron with dimension 0.13 × 0.09 × 0.07 mm^3 for **4** were selected. According to the systematic absences, **3** crystallizes in $P2_1/n$ and **4** in *C*2/*c*. All atoms in both compounds were subsequently refined with anisotropic displacement parameters.

Technical details of the data acquisition as well as some refinement results for all compounds are summarized in Table 1. Selected bond lengths and angles are given in Tables 2−5.

Further details of the crystal structure investigation can be obtained from the Fachinformationszentrum Karlsruhe, 76344 Eggenstein-Leopoldshafen, Germany, (fax: (49) 7247−808−666; E-mail: crysdata@fiz-karlsruhe.de) on quoting the depository number CSD-41911 ($K_9Nd[PS_4]_4$), CSD-41913 ($K_3Nd[PS_4]_2$), CSD-41912 ($Cs_3Nd[PS_4]_2$), CSD-41914 ($K_3Nd_3[PS_4]_4$).

Infrared Spectroscopy

Infrared spectra in the mid infrared (MIR) region (4000−400 cm^{-1}, 2 cm^{-1} resolution, 293 K) were recorded on a Genesis FT-spectrometer (ATI Mattson). The samples were ground with dry KBr into fine powders and pressed into transparent pellets. Infrared spectra in the far infrared

(25) Sheldrick, G. M. *SHELXTL*, version 5.10; Bruker Analytical X-ray Instruments, Inc.: Madison, WI, 1998.

(26) Spek, A. L. *J. Appl. Crystallogr.* **2003**, *36*, 7–13.

Table 2. Selected Bond Lengths (Å) and Angles (deg) for $K_9Nd[PS_4]_4$

Environment of Nd			
Nd(1)−S(3) × 2	3.0557(10)	S(3)−Nd(1)−S(3)	150.63(4)
Nd(1)−S(7) × 2	3.0584(11)	S(3)−Nd(1)−S(7)	124.10(3)
Nd(1)−S(4) × 2	3.0637(13)	S(7)−Nd(1)−S(7)	150.61(3)
Nd(1)−S(8) × 2	3.0689(13)	S(7)−Nd(1)−S(4)	123.57(3)
		S(3)−Nd(1)−S(8)	123.46(3)
		S(4)−Nd(1)−S(8)	171.68(2)
Nd(2)−S(2) × 2	3.1085(11)	S(2)−Nd(2)−S(2)	149.70(4)
Nd(2)−S(6) × 2	3.1091(11)	S(2)−Nd(2)−S(6)	123.00(3)
Nd(2)−S(8) × 2	3.1681(14)	S(6)−Nd(2)−S(6)	149.51(4)
Nd(2)−S(4) × 2	3.1697(14)	S(2)−Nd(2)−S(8)	123.78(3)
		S(6)−Nd(2)−S(4)	123.80(3)
		S(8)−Nd(2)−S(4)	171.95(2)
Environment of P			
P(1)−S(1)	2.0218(13)	S(1)−P(1)−S(2)	110.37(6)
P(1)−S(2)	2.0287(14)	S(1)−P(1)−S(3)	111.23(6)
P(1)−S(3)	2.0394(14)	S(1)−P(1)−S(4)	111.76(6)
P(1)−S(4)	2.0552(13)	S(2)−P(1)−S(3)	108.18(6)
		S(2)−P(1)−S(4)	109.13(6)
		S(3)−P(1)−S(4)	106.00(6)
P(2)−S(5)	2.0239(13)	S(5)−P(2)−S(6)	110.31(6)
P(2)−S(6)	2.0290(14)	S(5)−P(2)−S(7)	111.22(6)
P(2)−S(7)	2.0363(14)	S(5)−P(2)−S(8)	111.77(6)
P(2)−S(8)	2.0559(13)	S(6)−P(2)−S(7)	108.22(6)
		S(6)−P(2)−S(8)	109.03(3)
		S(7)−P(2)−S(8)	106.13(6)

Table 3. Selected Bond Lengths (Å) and Angles (deg) for $K_3Nd[PS_4]_2$

Environment of Nd			
Nd(1)−S(6)	2.8560(17)	S(6)−Nd(1)−S(7)	143.37(5)
Nd(1)−S(7)	2.9029(16)	S(2)−Nd(1)−S(8)	134.40(5)
Nd(1)−S(2)	2.9340(18)	S(6)−Nd(1)−S(4)	143.07(5)
Nd(1)−S(8)	2.9469(19)	S(2)−Nd(1)−S(4)	124.91(5)
Nd(1)−S(4)	2.9556(15)	S(7)−Nd(1)−S(4)	133.98(5)
Nd(1)−S(4)	3.0265(18)	S(8)−Nd(1)−S(4)	135.85(5)
Nd(1)−S(3)	3.1567(19)	S(7)−Nd(1)−S(3)	124.30(4)
Nd(1)−S(8)	3.2307(18)	S(2)−Nd(1)−S(3)	132.08(5)
		S(3)−Nd(1)−S(8)	147.72(5)
Environment of P			
P(1)−S(1)	1.996(2)	S(1)−P(1)−S(2)	111.60(10)
P(1)−S(2)	2.033(2)	S(1)−P(1)−S(3)	117.68(12)
P(1)−S(3)	2.041(2)	S(1)−P(1)−S(4)	111.33(10)
P(1)−S(4)	2.059(2)	S(2)−P(1)−S(3)	108.62(11)
		S(2)−P(1)−S(4)	104.64(10)
		S(3)−P(1)−S(4)	101.82(9)
P(2)−S(5)	2.008(2)	S(5)−P(2)−S(6)	110.42(10)
P(2)−S(6)	2.035(2)	S(5)−P(2)−S(7)	109.53(10)
P(2)−S(7)	2.042(2)	S(5)−P(2)−S(8)	112.65(10)
P(2)−S(8)	2.066(2)	S(6)−P(2)−S(7)	109.44(10)
		S(6)−P(2)−S(8)	108.91(11)
		S(7)−P(2)−S(8)	105.75(9)

(FIR) region (550−80 cm^{-1}) were collected on an ISF-66 device (Bruker) with finely powdered samples pressed in polyethylene pellets.

Raman Spectroscopy

FT-Raman spectra were recorded on an ISF-66 spectrometer (Bruker) equipped with an additional FRA 106 Raman module and a diode-pumped Nd/YAG laser ($\lambda = 1064$ nm; Adlas). Finely powdered samples were pressed into the small hole of Al sample holders. The measuring range was −2500 to 3500 cm^{-1} with a resolution of 2 cm^{-1} at 293 K. Conventional Raman spectra were measured on a multichannel XY Spectrometer (Dilor) equipped with a nitrogen cooled CCD detector. Excitation of the Raman spectra was obtained by selected laser lines of an Ar^+/Kr^+ laser type (Spectra Physics). The finely powdered sample was mixed with KBr and pressed into a pellet that is fixed on a vibrating sample holder cooled at about 15 K by a closed cycle He refrigerator (Model 22/8300, CTI) as described elsewhere[27] to prevent heating of the sample. The spectra have not been corrected for spectrometer and detector response.

Table 4. Selected Bond Lengths (Å) and Angles (deg) for $Cs_3Nd[PS_4]_2$

Environment of Nd			
Nd(1)−S(8)	2.8766(13)	S(8)−Nd(1)−S(2)	100.66(4)
Nd(1)−S(3)	2.8792(14)	S(3)−Nd(1)−S(2)	142.05(4)
Nd(1)−S(2)	2.9041(13)	S(8)−Nd(1)−S(4)	141.03(4)
Nd(1)−S(4)	2.9312(13)	S(8)−Nd(1)−S(1)	138.79(4)
Nd(1)−S(1)	2.9321(13)	S(3)−Nd(1)−S(1)	129.48(4)
Nd(1)−S(7)	2.9473(12)	S(2)−Nd(1)−S(7)	139.88(4)
Nd(1)−S(4)	3.0655(12)	S(4)−Nd(1)−S(7)	118.91(4)
Nd(1)−S(6)	3.1698(15)	S(1)−Nd(1)−S(4)	135.01(4)
		S(7)−Nd(1)−S(4)	137.70(3)
Environment of P			
P(1)−S(1)	2.0361(17)	S(1)−P(1)−S(2)	109.50(8)
P(1)−S(2)	2.0424(17)	S(1)−P(1)−S(3)	109.52(7)
P(1)−S(3)	2.0445(18)	S(1)−P(1)−S(4)	114.72(7)
P(1)−S(4)	2.0535(17)	S(2)−P(1)−S(3)	111.12(7)
		S(2)−P(1)−S(4)	105.62(7)
		S(3)−P(1)−S(4)	106.30(7)
P(2)−S(5)	2.0057(19)	S(5)−P(2)−S(6)	117.86(9)
P(2)−S(6)	2.0431(19)	S(5)−P(2)−S(7)	112.21(8)
P(2)−S(7)	2.0512(17)	S(5)−P(2)−S(8)	111.28(8)
P(2)−S(8)	2.0594(17)	S(6)−P(2)−S(7)	104.04(7)
		S(6)−P(2)−S(8)	103.57(7)
		S(7)−P(2)−S(8)	106.96(8)

Table 5. Selected Bond Lengths (Å) and Angles (deg) for $K_3Nd_3[PS_4]_4$

Environment of Nd			
Nd(1)−S(2)	2.8236(11)	S(2)−Nd(1)−S(3)	141.15(3)
Nd(1)−S(3)	2.8461(12)	S(3)−Nd(1)−S(8)	110.13(3)
Nd(1)−S(5)	2.8475(11)	S(5)−Nd(1)−S(8)	144.10(3)
Nd(1)−S(8)	2.8800(11)	S(3)−Nd(1)−S(7)	141.86(3)
Nd(1)−S(7)	2.9852(11)	S(5)−Nd(1)−S(4)	145.75(3)
Nd(1)−S(4)	3.0241(10)	S(2)−Nd(1)−S(7)	140.99(3)
Nd(1)−S(7)	3.0491(11)	S(4)−Nd(1)−S(7)	112.87(3)
Nd(1)−S(4)	3.0826(11)	S(8)−Nd(1)−S(4)	133.92(3)
Nd(2)−S(6) × 2	2.8980(11)	S(7)−Nd(1)−S(4)	129.84(3)
Nd(2)−S(1) × 2	2.8984(11)	S(1)−Nd(2)−S(1)	148.40(4)
Nd(2)−S(8) × 2	2.9183(10)	S(6)−Nd(2)−S(8)	140.70(3)
Nd(2)−S(4) × 2	3.0546(10)	S(1)−Nd(2)−S(8)	110.10(3)
		S(8)−Nd(2)−S(8)	149.88(4)
Environment of P			
P(1)−S(1)	2.0170(15)	S(1)−P(1)−S(2)	111.52(7)
P(1)−S(2)	2.0299(16)	S(1)−P(1)−S(3)	110.83(7)
P(1)−S(3)	2.0350(14)	S(1)−P(1)−S(4)	106.45(6)
P(1)−S(4)	2.0810(15)	S(2)−P(1)−S(3)	109.56(7)
		S(2)−P(1)−S(4)	107.72(6)
		S(3)−P(1)−S(4)	110.69(6)
P(2)−S(5)	2.0253(16)	S(5)−P(2)−S(6)	111.92(7)
P(2)−S(6)	2.0283(14)	S(5)−P(2)−S(7)	109.61(6)
P(2)−S(7)	2.0464(15)	S(5)−P(2)−S(8)	109.54(7)
P(2)−S(8)	2.0659(15)	S(6)−P(2)−S(7)	109.85(7)
		S(6)−P(2)−S(8)	107.83(6)
		S(7)−P(2)−S(8)	107.99(6)

Solid-State Ultraviolet (UV)-Visible(vis)-Near-IR Spectroscopy. UV/vis/NIR diffuse reflectance spectra at 293 K were recorded on a Cary 5 spectrometer (Varian Techtron Pty.). The spectrometer was equipped with an Ulbricht sphere (Diffuse reflectance accessory; Varian Techtron Pty.). The inner wall of the Ulbricht sphere (diameter 110 mm) was covered with a PTFE layer of 4 mm thickness. A PbS detector (NIR) and a photomultiplier (UV/vis) were attached to the Ulbricht sphere.

The samples were ground together with $BaSO_4$ and prepared as a flat specimen. Resolution was 1 nm for the

(27) Preetz, W.; Parzich, E. *Z. Naturforsch.* **1993**, *48b*, 1737–1741.

UV/vis range and 2 nm for the NIR range. The measuring range was 250−2000 nm. $BaSO_4$ was used as standard for 100% reflectance. Absorption data were calculated from the reflectance data using the Kubelka−Munk function.[28] The approximate band gap was determined as the intersection point between the energy axis and the line extrapolated from the linear part of the absorption edge in a $(F(R))^2$ versus energy plot.

3. Results and Discussion

3.1. Synthesis. Syntheses of compounds **1** and **4** were achieved by reacting mixtures of K_2S_3/Nd/P_2S_5/S at 973 K in 1:1:1:6 and 2:1:0.5:6 molar ratios, respectively. **1** was obtained as transparent pale red platelets and **4** as colorless platelets. The reactions involve the oxidative dissolution of Nd in the basic melt and the subsequent coordination of the trivalent Nd cations by the $[PS_4]^{3-}$ anions. The reaction parameters were varied by changing the amounts of K_2S_3 and P_2S_5. Increasing the basicity of the flux by increasing K_2S_3 and decreasing P_2S_5, led to the formation of compound **1**. All attempts to obtain **1** in higher yields were unsuccessful, and the products always contained some amount of compound **2**.

Compounds **2** and **3** were isolated from reaction mixtures containing BaS or As_2S_3, respectively. With theses syntheses the possibility of the formation of mixed Nd alkali-metal alkaline-metal (Ba) thiophosphates and Nd alkali-metal thiophosphate-thioarsenate compounds via the flux method was explored. **2** was obtained in a reasonable yield by reacting a mixture of K_2S_3/BaS/Nd/P_2S_5/S with molar ratio of 2:0.25:1:1:6. On increase of the fraction of BaS, the two compounds $KBaPS_4$ and NdS_2 (EDX) were identified as main products. The reactions with SrS and CaS were also explored. Under the same reaction conditions, $KSrPS_4$ ($KCaPS_4$) and NdS_2 (EDX) could be identified.

3 was obtained applying a mixture Cs_2S_3/Nd/P_2S_5/As_2S_3/S (molar ratio 2:1:1:0.5:6). Increasing the fraction of As_2S_3 led to the formation of yellow glassy products along with **3**. After these syntheses several experiments were performed in the Cs_2S_3/Nd/P_2S_5/S system. The best results with a yield of about 90% were obtained using Cs_2S_3/Nd/P_2S_5/S in a molar ratio of 2:1:1:6.

3.2. Crystal Structures. $K_9Nd[PS_4]_4$ (**1**) crystallizes in the monoclinic space group *C*2/*c* with two crystallographically independent P, four unique K, eight unique S atoms that are located on general positions. The two unique Nd atoms are also on general sites which show a mixed occupancy with K cations. The structure of $K_9Nd[PS_4]_4$ (**1**) is depicted in Figure 1 and can be viewed as an ordering variant of the $K_9Ce[PS_4]_4$ structure type,[10] which possesses a 2-fold axis along [001] as twinning element.

Compared to the Ce compound where only 3% of K^+ are located on the Ce^{3+} positions and vice versa, $K_9Nd[PS_4]_4$ (**1**) shows a more complicated mixed-cation occupation pattern. Both Nd^{3+} ions are coordinated by eight S atoms through four edge-sharing $[PS_4]$ tetrahedra to form trigonal dodecahedra. The Nd−S distances range from 3.0557(10) to 3.0689(13) Å for Nd(1) and 3.1085(11) to 3.1697(14) Å for Nd(2) (see Table 2). The average of 3.06 Å for Nd(1)−S and 3.14 Å for Nd(2)−S are longer than the average Nd−S distances of 2.96 Å in $NdPS_4$[2a,f] and of 3.00 Å in $K_3Nd[PS_4]_2$ (see below). The trigonal dodecahedra share common edges with $[PS_4]$ tetrahedra forming $^1_\infty\{Nd(PS_4)_2\}^{3-}$ chains (Figure 2).

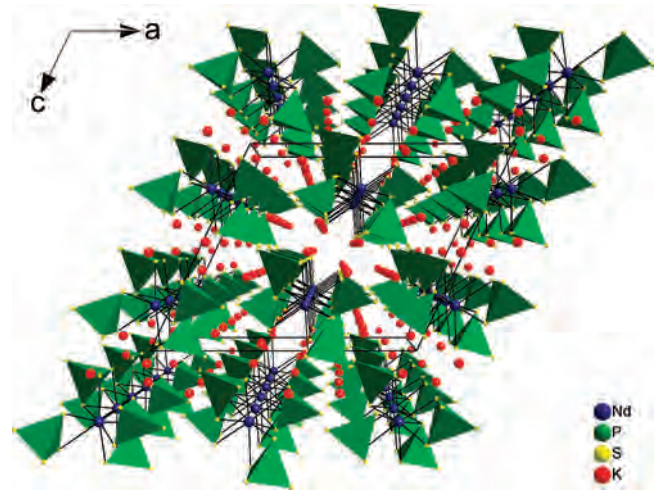

Figure 1. Crystal structure of $K_9Nd[PS_4]_4$ with perspective view along [010].

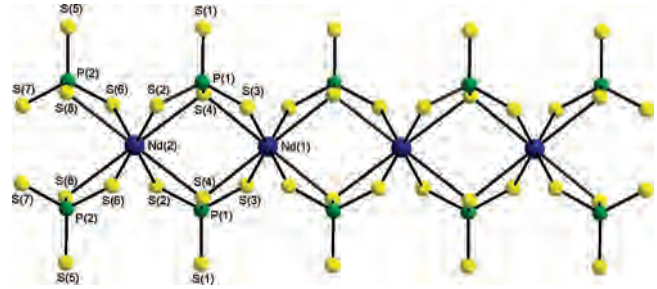

Figure 2. Interconnection of the $\{Nd[PS_4]_4\}$ units into chains with atomic labeling.

But because of the statistical occupation of Nd and K sites, isolated $\{Nd[PS_4]_4\}^{9-}$ units occur occasionally. The chains are separated by the four crystallographically distinct K^+ cations, which are coordinated in an irregular environment by 8 or 10 S atoms with distances from 3.2291(15) to 3.9981(14) Å.

$K_3Nd[PS_4]_2$ (**2**) (see Figure 3) crystallizes in the monoclinic space group $P2_1/c$ with one crystallographically independent Nd, two unique P, three unique K, and eight unique S atoms that are located on general positions.

2 contains linear chains formed by bicapped $\{NdS_8\}$ trigonal prisms which are joined through edge sharing with neighboring $\{NdS_8\}$ polyhedra and with $[PS_4]^{3-}$ tetrahedra. Figure 4 displays the coordination around the Nd^{3+} ions in the chain running along the *a*-axis. All eight S atoms bound to one Nd^{3+} are part of $[PS_4]^{3-}$ anions. The Nd−S bond lengths range from 2.8560(17) to 3.2307(18) Å with an average of 3.00 Å (Table 3). The two longest distances in the $\{NdS_8\}$ polyhedron at 3.1568(19) and 3.2307(18) Å are to the capping S atoms (S(3) and S(8), see Figure 4), respectively. Each $\{NdS_8\}$ polyhedron shares two of its edges

(28) Kulbelka, P.; Munk, F. *Z. Tech. Phys.* **1931**, *12*, 593–601.

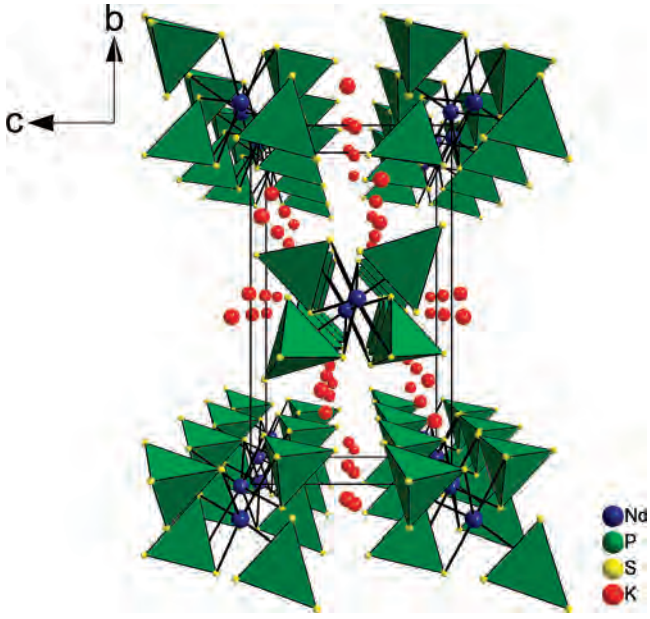

Figure 3. Perspective view of $K_3Nd[PS_4]_2$ (**2**) crystal structure down [100].

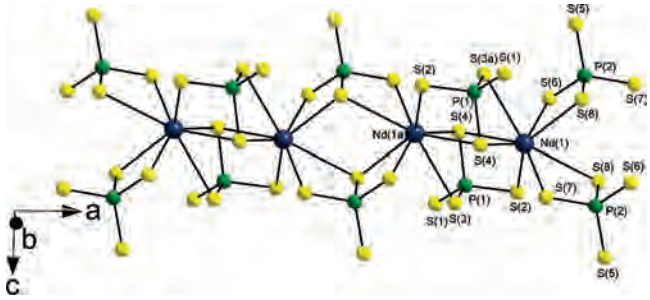

Figure 4. Perspective view of the $\{Nd[PS_4]_2\}^{3-}$ chain. The $\{NdS_8\}$ polyhedra are linked to each other through edge sharing to form an infinite chain along [100].

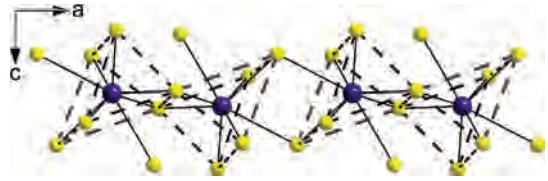

Figure 5. Interconnection of the $\{NdS_8\}$ polyhedra in $K_3Nd[PS_4]_2$. Dashed black lines highlight the polyhedra. $[PS_4]$ groups are omitted for clarity.

(S(4)−S(4) and S(8)−S(8)) with two other polyhedra on opposite sides of the polyhedra to form $^1_\infty\{Nd(PS_4)_2\}^{3-}$ chains.

This connection scheme is responsible for the kink-like shape of the chains as depicted in Figure 5.

The two distinct $[PS_4]^{3-}$ anions are each coordinated to Nd^{3+} ions by one S atom (S(2), S(3) for P(1) and S(6), S(7) for P(2)) for each neighboring Nd^{3+}, whereas the third S atom (S(4) and S(8)) acts as a bridge to both Nd^{3+}. The fourth S atom of each thiophosphate anion (S(1) and S(5)) remains terminal. An obvious difference of the two $[PS_4]^{3-}$ anions is their orientation with respect to the chain axis. The $[P(1)S_4]$ tetrahedron shares two edges with $\{NdS_8\}$ polyhedra, with the Nd(1)−S(4)−Nd(1) angle of 90.71(5)°. The $[P(2)S_4]$ tetrahedron has also two common edges with neighboring $\{NdS_8\}$ polyhedra, but the trigonal face of the tetrahedron is almost parallel to the chain axis resulting in an almost perfect tetrahedral angle of 108.86(5)° for Nd(1)−S(8)−Nd(1) around the bridging S(8) atom. The different orientations of the tetrahedra lead to two different Nd−Nd distances. For Nd−Nd bridged by S(8) the separation of 5.0276(6) Å is significantly larger than that with the S(4) bridge of 4.2564(6) Å. Both separations are slightly shorter than that in $Nd[PS_4]$ (5.420 Å)[2f] but much longer than the sum of the ionic radius of Nd^{3+} (1.109 Å).[33] The P−S bond lengths and bond angles vary depending on how S atoms are bound to Nd^{3+}. In $[P(1)S_4]$, the P(1)−S(1) bond length is 1.996(2) Å with corresponding S(1)−P(1)−S(2)/(3)/(4) angles of 111.60(10)°, 117.68(12)°, and 111.33(10)°, respectively, while the P(1)−S(2)/(3)/(4) bonds are longer with 2.033(2), 2.041(2), 2.059(2) Å and the corresponding angles are obviously smaller (S(2)−P(1)−(3): 108.62(11)°, S(2)−P(1)−S(4): 104.64(10)°, S(3)−P(1)−S(4): 101.82(9)°). These differences of the bond lengths and angles may be a result of the partial double bond character of the terminal P(1)−S(1) bond. The same trend is observed for $[P(2)S_4]$, with P(2)−S(5) being shorter (2.008(2) Å) than P(2)−S(6)/(7)/(8) (2.035(2), 2.042(2), 2.066(2) Å), whereas S(5)−P(2)−S(6)/(7)/(8) bond angles (110.42(10)°, 109.53(10)°, 112.65(10)°) are larger than S(6, 7, 8)−P(2)−S(6, 7, 8) (e.g., S(7)−P(2)−S(8): 105.75(9)°) (Table 3). The charge compensating K^+ ions reside in the voids between the $\{Nd[PS_4]_2\}^{3-}$ chains, where the shortest interchain S−S distance is 3.760(2) Å. All K cations are in an irregular coordination environment of nine S atoms with K−S distances from 3.147(2) to 3.980(3) Å.

The structure of compound **2** can be compared with that of $K_3La[PS_4]_2$[12] and $K_3Ce[PS_4]_2$.[9] A common feature of the three structures is an alternating short−long metal to metal separation along the one-dimensional chains. The La−La distances in $K_3La[PS_4]_2$ are 5.045(2) and 4.217(2) Å whereas the analogous Ce−Ce separations in $K_3Ce[PS_4]_2$ amount to 5.022(1) and 4.211(1) Å. In the La/Ce compounds the rare earth ions are surrounded by nine S atoms with average bond lengths of 3.076(2) (La) and 3.058(2) (Ce), whereas in **2** Nd^{3+} is in an environment of eight S atoms with a mean Nd−S bond length of 3.001(3) Å. The different coordination numbers in the three compounds is caused by the different orientations of the bridging $[PS_4]$ tetrahedra along the chains. As can be seen in Figure 4, the $P(1)S_4$ tetrahedron is turned away from the $\{NdS_8\}$ polyhedron so that the distance between Nd(1) and S(3) is enlarged to 3.479(2) Å. In $K_3La[PS_4]_2$ and $K_3Ce[PS_4]_2$, the corresponding distances are 3.118(2) and 3.149(2) Å, being reasonably short for bonding interactions and the formation of LaS_9/CeS_9 polyhedra.

Despite the identical ratio of alkali ions to Nd^{3+} and thiophosphate ions, $Cs_3Nd[PS_4]_2$ (**3**) crystallizes with a different one-dimensional anionic structure type. The main structural feature is a $^1_\infty\{Nd[PS_4]_2\}^{3-}$ zigzag chain running along the crystallographic *b*-axis which is displayed in Figure 6.

The chain contains one independent Nd^{3+} ion but two different bridging $[PS_4]^{3-}$ units. The $[P(1)S_4]^{3-}$ group has bonds to three Nd^{3+} acting as a bridging unit while the $[P(2)S_4]^{3-}$ tetrahedron is only attached to one Nd atom via

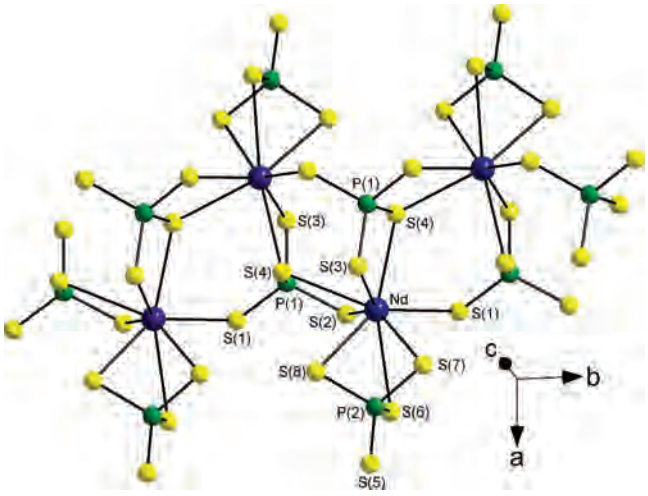

Figure 6. Perspective view of the $Nd[PS_4]_2^{3-}$ anionic chain in $Cs_3Nd[PS_4]_2$.

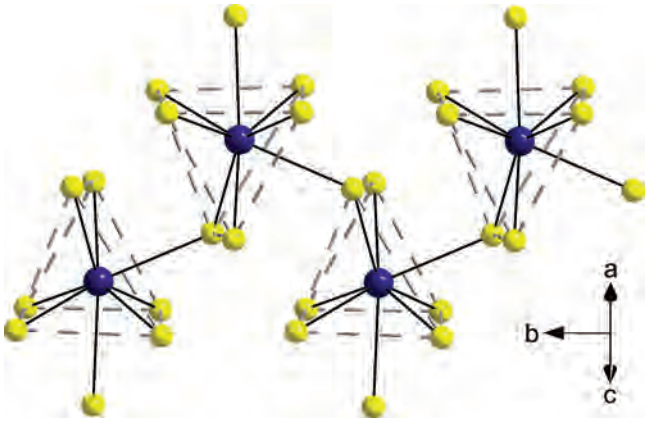

Figure 7. Interconnection of $\{NdS_8\}$ polyhedra in **3**. Dashed lines highlight the polyhedra. $[PS_4]^{3-}$ anions are omitted for clarity.

three S atoms. The anionic chains are well separated by Cs^+ cations.

In contrast to the linear chain in compound **2**, the bicapped $\{NdS_8\}$ trigonal prisms in **3** are linked by common corners μ_2-S(4) of $[P(1)S_4]$, and the three remaining S atoms of $[P(1)S_4]$ have each only one bond to a Nd^{3+} ion. Hence, the $[P(1)S_4]$ tetrahedron has one common corner (S(1)) with one $\{NdS_8\}$ polyhedron and two edges (S(2)−S(4) and S(3)−S(4)) with the other two $\{NdS_8\}$ polyhedra. The Nd−S−Nd angle around the μ_2-S(4) atom is 125.90°. The basal planes of bicapped $\{NdS_8\}$ trigonal prisms are nearly parallel to the chain direction and perpendicular to the [101] direction (Figure 7).

The Nd−S bonds range from 2.8766(13) to 3.1698(15) Å with an average of 2.96 Å. Like in the other compounds the bond lengths to capping atoms S(4) and S(6) are obviously longer. (Nd−S(4): 3.0655(12) Å and Nd−S(6): 3.1698(15) Å). The $[P(2)S_4]$ tetrahedron shares one triangular face with one $\{NdS_8\}$ polyhedron, and the fourth S atom (S(5)) remains terminal. The P−S bond lengths (2.0057(19)−2.0594(17) Å; average: 2.042 Å) show a clearly more narrow distribution than those in **2**. The P(1)−S bonds range from 2.036(2) to 2.054(2) Å and the deviations of the S−P−S bond angles from the ideal tetrahedral value are small (105.6(1)°−114.7(1)°) (see Table 4). In contrast, the P(2)−S bonds scatter over a larger range (P(2)−S: 2.006(2)−2.059(2) Å), and the angles S−P(2)−S (103.6(1)−117.9(1)°) indicate a more severe distortion of the tetrahedron. Again, the shortest bond length is found to the terminal atom S(5). The chains are separated by Cs^+ cations residing on three different sites. All Cs atoms are coordinated by nine S atoms in an irregular environment with Cs−S distances from 3.4255(13) to 3.8917(15) Å.

$K_3Nd_3[PS_4]_4$ (**4**) crystallizes in the monoclinic space group *C*2/*c* with two crystallographically independent Nd, K, P, and eight unique S atoms. In the structure two different $\{NdS_8\}$ polyhedra share edges with four $[PS_4]^{3-}$ tetrahedra. The Nd(1) atom is surrounded by eight S atoms yielding a bicapped trigonal prism. The $\{Nd(1)S_8\}$ polyhedra are linked by common edges of neighboring $\{Nd(1)S_8\}$ polyhedra building a straight $^1{}_\infty\{Nd(1)[PS_4]_2\}^{3-}$ chain running along [110] and [$\bar{1}$10] as shown in Figure 8a,b.

The Nd(2) atom is also surrounded by eight S atoms of four edge sharing $[PS_4]$ tetrahedra, but in this case a trigonal dodecahedron is formed (Figure 8c). The $\{Nd(2)S_8\}$ polyhedra join the $^1{}_\infty\{Nd(1)[PS_4]_2\}^{3-}$ chains via common corners into a three-dimensional network $^3{}_\infty\{Nd_3[PS_4]_4\}^{3-}$ (Figure 9), with the tunnels running parallel to [110] and [$\bar{1}$10]. The dimension of the tunnels is about 26.6 × 6.2 Å measured from coordinate to coordinate.

The Nd−S bonds (2.8236(11)−3.0491(11) Å for Nd(1); 2.8980(11)−3.0546(10) Å for Nd(2); average for both: 2.94 Å) are in the range observed in literature[2a,f,15,21] and also in the other three compounds. Five Nd(1)−S and six Nd(2)−S distances are relatively short and below 3.0 Å (Table 5). The remaining Nd−S bonds (Nd(1)−S(4), Nd(1)−S(7); Nd(2)−S(4)) are significantly longer (Table 5). The P−S bond lengths range from 2.0170(15) to 2.0810(15) Å for $[P(1)S_4]$ and from 2.0253(16) to 2.0659(15) Å for $[P(2)S_4]$ (Table 5) with corresponding angles (106.45(6)−111.52(7)° for $[P(1)S_4]$; 107.83(6)−111.92(7)° for $[P(2)S_4]$) which indicate only a slight deviation from the ideal tetrahedral geometry. The cationic surrounding of the $[P(1)S_4]$ and $[P(2)S_4]$ tetrahedra is almost identical. Both share three edges with two $\{Nd(1)S_8\}$ bicapped trigonal prisms and one $\{Nd(2)S_8\}$ trigonal dodecahedron and three K cations. The K(1) ion is located at the tunnel edges having contacts to eight S atoms in an irregular environment with K−S distances ranging from 3.209(2) to 3.588(2) Å (average: 3.37 Å). The K(2) ion is situated at the center of the tunnel in a distorted cubic environment with K(2)−S distances between 3.190(1) and 3.368(1) Å (average: 3.28 Å). Compared to the Nd, P, and S atoms, the K^+ ions have larger displacement parameters which may be due to a partial static disorder caused by a relatively poor fit of the ionic radius of K^+ and the dimensions of the tunnel.

Although many complex rare earth thiophosphates have been synthesized and characterized during the past decade, only few of these compounds crystallize with three-dimensional anionic frameworks. Compounds with anionic chains are $K_3Ce[PS_4]_2$, $K_3La[PS_4]_2$ and the selenides $K_3La[PSe_4]_2$,[12b] $Rb_3Ce[PSe_4]_2$, and $Cs_3Gd[PSe_4]_2$,[8] which are

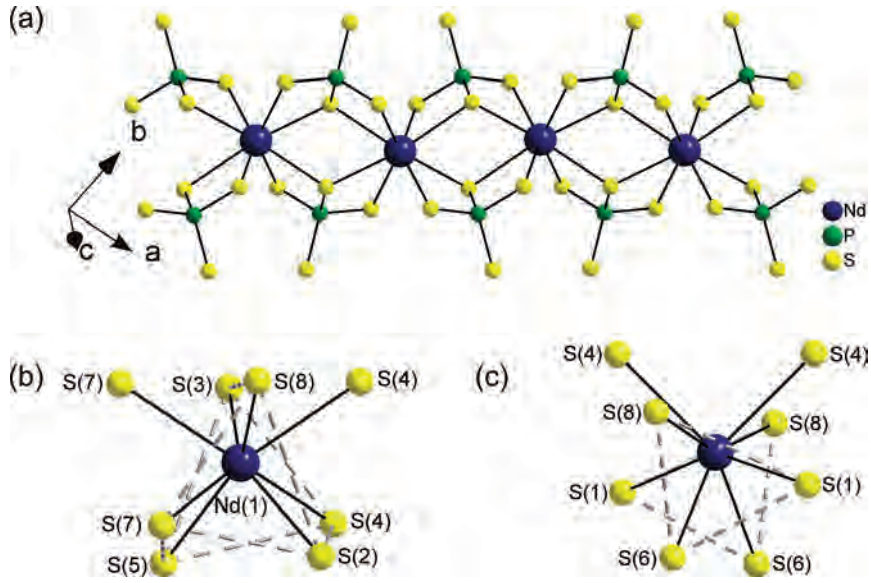

Figure 8. (a) Section of the $^1_\infty\{Nd(1)[PS_4]_2\}^{3-}$ chain in $K_3Nd_3[PS_4]_4$. The $\{NdS_8\}$ polyhedra are linked via edge sharing to form an infinite chain along [110] and [$\bar{1}$10]. (b) View of the $\{Nd(1)S_8\}$ bicapped trigonal prism. The trigonal prism is outlined with dashed lines for clarity. The long bonds are to the capping atoms S(4) and S(7); (c) View of the $\{Nd(2)S_8\}$ trigonal dodecahedron. Two basal triangles are outlined with dashed lines.

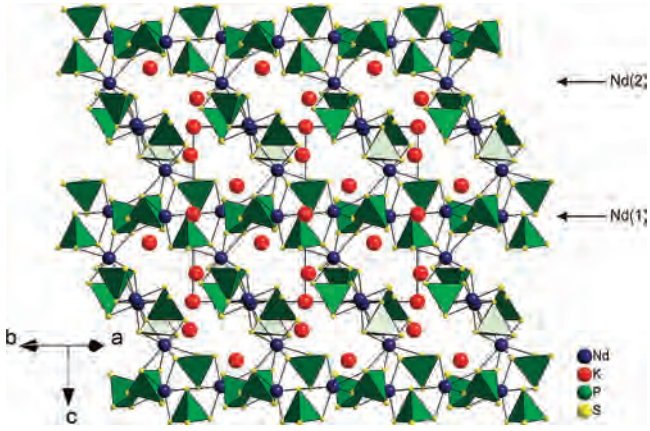

Figure 9. View of the structure of $K_3Nd_3[PS_4]_4$ with view along [110].

isostructural to $K_3Pu[PS_4]_2$,[29] while three-dimensional networks were reported for $LiEuPQ_4$ (Q = S, Se)[2i,11] $Cs_3Pr_5[PS_4]_6$,[19] and $K_6Yb_3[PS_4]_5$.[18] The anionic chains in $A_3Ln[PQ_4]_2$ (A = alkali metal, Q = S, Se) are very similar to that of compound **2** but distinctly different from the chains observed for **3**. In **2** and the above-mentioned compounds, the Ln^{3+} ions are in bicapped trigonal prismatic chalcogen coordination and the linkage between the prisms and the two crystallographically independent tetrahedral $[PQ_4]$ groups lead to the formation of linear chains, whereas zigzag chains are formed in compound **3**. The only other example of this formula type with zigzag chains is $K_3Bi[PS_4]_2$.[30] Its polar character is more pronounced because of the steric effect of the lone pair of the Bi(III) ion. The recently reported thioarsenates $K_3Ln[AsS_4]_2$ (Ln = Nd, Sm, Gd)[31] are characterized by linear anions showing a relation to the anions in compound **2**.

While $Rb_3Pr_3[PS_4]_4$, $Rb_3Er_3[PS_4]_4$,[17] and $K_3Nd_3[PS_4]_4$ have the same formulas, three different structures with two different dimensionalities are observed. One important difference between the structures is the arrangement and orientation of $^1_\infty\{Ln[PS_4]_2\}^{3-}$ chains. In $K_3Nd_3[PS_4]_4$ there are two types of $^1_\infty\{Nd(1)[PS_4]_2\}^{3-}$ chains: a $^1_\infty\{Nd(1)[PS_4]_2\}^{3-}$ chain along the [110] direction and a $^1_\infty\{Nd(1)[PS_4]_2\}^{3-}$ chain along [$\bar{1}$10]. The $^1_\infty\{Nd(1)[PS_4]_2\}^{3-}$ chains running along [110] can be viewed as pseudolayers at $z \approx 0$, whereas the $^1_\infty\{Nd(1)[PS_4]_2\}^{3-}$ chains along [$\bar{1}$10] form pseudolayers at $z \approx 0.5$ as shown in Figure 10. Both are linked by $\{Nd(2)S_8\}$ polyhedra at $z \approx 0.25$ and 0.75 to form the three-dimensional framework. But in $Rb_3Er_3[PS_4]_4$ there is only one type of $^1_\infty\{Er(2,3)[PS_4]_2\}^{3-}$ chain, which is running parallel to [100]. The $^1_\infty\{Er(2,3)[PS_4]_2\}^{3-}$ chains at $y \approx 0.25$ and 0.75 are connected by $\{Er(1)S_8\}$ polyhedra at $y \approx 0.25$ and 0.75 to form two different two-dimensional $^2_\infty\{Er_3[PS_4]_4\}^{3-}$ layers, respectively. On the other hand, the dimensionality of anionic frameworks increases as the alkali metal cation size decreases which is the well-known counterion effect.[32] In the three structures this effect takes place because of the size differences between K^+ (1.51 Å (CN = 8)) and Rb^+ (1.61 Å (CN = 8)). The size of K^+ in $K_3Nd_3[PS_4]_4$ (**4**) is smaller than that of Rb^+ in $Rb_3Pr_3[PS_4]_4$ and $Rb_3Er_3[PS_4]_4$, allowing a denser packing of the anionic part of the structures. But this density increase can only be realized when the volume of the anions is also reduced. Assuming a constant volume of the anionic part of the structure the replacement of the larger Rb^+ by the smaller K^+ should lead to a destabilization of the structure because of repulsive interanionic forces. The anionic volume can be decreased by increasing the connectivity of the atoms and

(29) Hess, R. F.; Gordon, P. L.; Tait, D.; Abney, K. D.; Dorhout, P. K. *J. Am. Chem. Soc.* **2002**, *124*, 1327–1333.
(30) McCarthy, T.; Kanatzidis, M. G. *J. Alloys Compd.* **1996**, *236*, 70–85.
(31) Wu, Y.-D.; Näther, C.; Bensch, W. *Inorg. Chem.* **2006**, *45*, 8835–8837.
(32) Kim, K.-W.; Kanatzidis, M. G. *J. Am. Chem. Soc.* **1998**, *120*, 8124–8135.
(33) Shannon, R. D. *Acta Crystallogr.* **1976**, *A32*, 751–767.

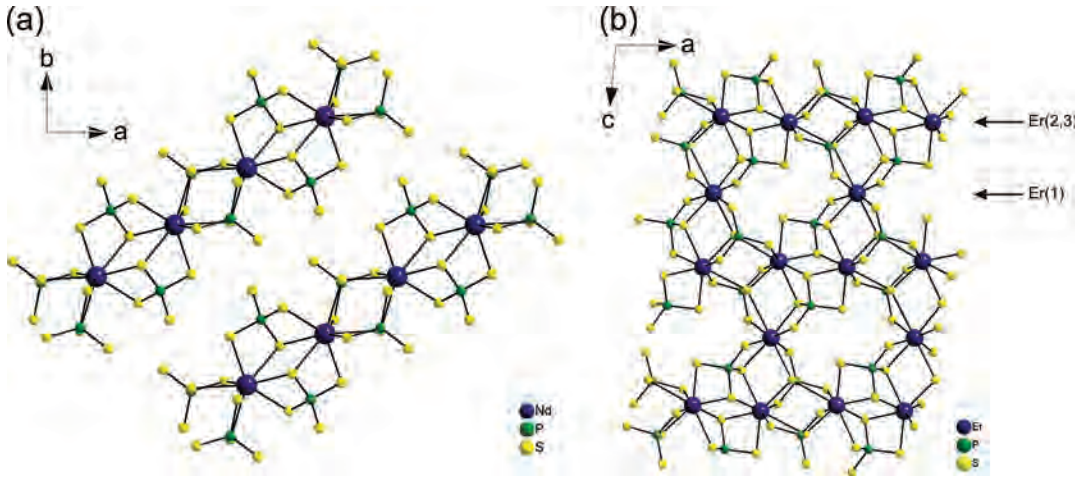

Figure 10. (a) View of the layer $^1_\infty\{Nd(1)[PS_4]_2\}^{3-}$ in **4** along [110]; (b) view of the $^2_\infty\{Er_3[PS_4]_4\}^{3-}$ layer down [010].

by association of discrete components into larger building units to increase the dimensionality. Therefore, the $\{Ln_3[PS_4]_4\}^{3-}$ framework in **4** is three-dimensional, whereas the anionic part of $Rb_3Pr_3[PS_4]_4$ and $Rb_3Er_3[PS_4]_4$ is two-dimensional.

3.3. Spectroscopic Properties. The IR and Raman spectra of **2**, **3**, and **4** are shown in Figure 11 jointly with the corresponding vibrational wavenumbers and their assignments based for simplicity on local T_d symmetry. The vibrational Raman spectra have been excited with two different wavelengths (488.0 and 496.5 nm) to discriminate them by their constant Raman shifts from potentially present luminescence spectra. No significant resonance Raman effect has been detected, and small differences in the intensity pattern between the different excitation wavelengths are instead presumed to result essentially from not corrected absorption.

For every alkali neodymium thiophosphate, the only vibrationally active species is the $[PS_4]^{3-}$ anion, and therefore their vibrational spectra are closely related. In the range from 200 to 650 cm^{-1} (Figure 11), bands attributed to the internal vibrations of the $[PS_4]^{3-}$ anion are observed, while those for rotations and translations of the $[PS_4]^{3-}$ anion and the cations in the crystal lattices are at lower energy. For experimental reasons, these external vibrations have not been studied systematically. According to the group theoretical selection rules for tetrahedral molecules with T_d symmetry, both totally symmetric and antisymmetric P−S stretching vibrations ν_1 and ν_3 of symmetry a_1 and t_2 and both S−P−S bending vibrations ν_2 and ν_4 of symmetry e and t_2, respectively, are observed in the Raman spectra as depicted in Figure 11. In the corresponding IR spectra only the vibrations $\nu_3 > \nu_4$ are observed. Thus, the coincidence of each IR band with its counterpart in the Raman spectrum in the region of the ν_3 (540−609 cm^{-1}) and ν_4 vibrations (242−302 cm^{-1}) confirms our assignment. The totally symmetric P−S vibration ν_1 in the range 419−444 cm^{-1} has the expected very high intensity in the Raman spectrum. It is almost missing in the IR spectrum, while ν_2 at about 207−237 cm^{-1} is only weak in the Raman and absent in the IR spectrum. The signature of present Raman spectra follows closely that found in the

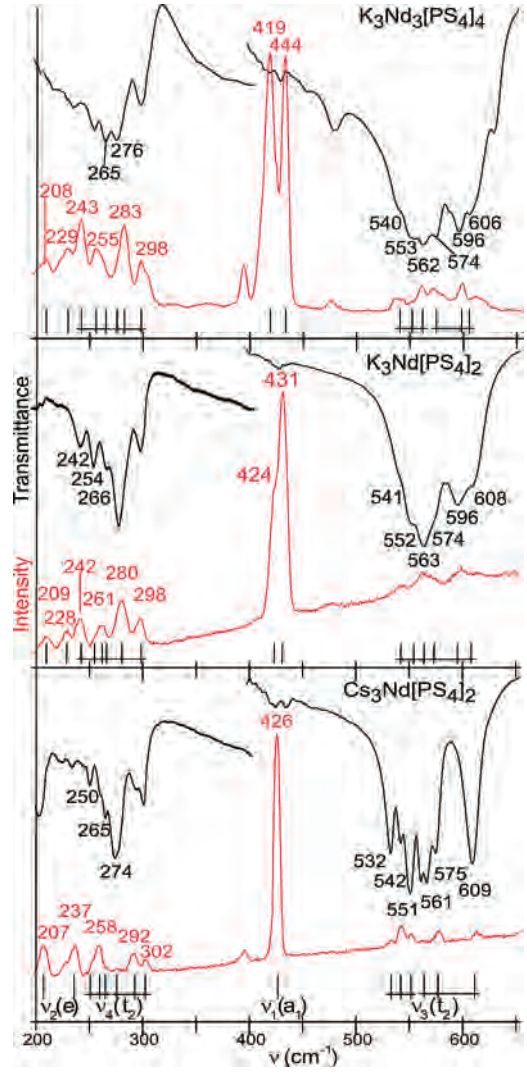

Figure 11. Comparison of the FIR/MIR (black; 293 K) and Raman spectra (red; λ_{exc} = 488 nm; ~15 K) of the $[PS_4]^{3-}$ anions of **2**−**4**.

Raman spectrum of the free $[PS_4]^{3-}$ anion dissolved in aqueous solution,[34] but most of the vibrational modes in **2**−**4**, especially ν_1 and ν_3, are shifted to higher wavenumbers

(34) Müller, A.; Mohan, N.; Cristophliemk, P.; Tossidis, I.; Dräger, M. *Spectrochim. Acta* **1973**, *29A*, 1345–1356.

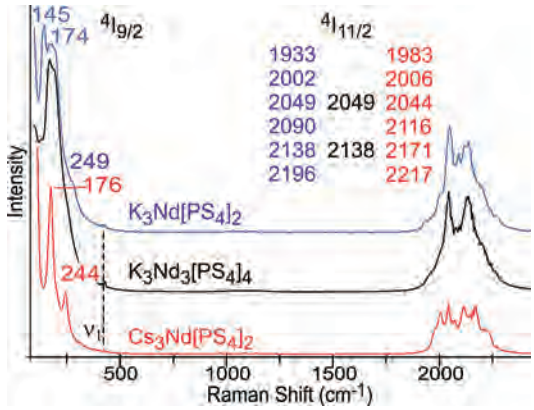

Figure 12. FT-Raman spectra (λ_{exc} = 1064 nm, 293 K) of **2**−**4** and assignment of the electronic Raman transitions from the ground level of the $^4I_{9/2}$ manifold to Stark levels of the $^4I_{9/2}$ and $^4I_{11/2}$ manifolds, respectively.

because of the tighter P−S binding in the solid state. As a consequence of the presence of two crystallographically unique phosphorus atoms in **2**−**4**, there is a set of the four internal vibrations for each $[PS_4]^{3-}$ anion, except for **3**, where both ν_1 modes apparently coincide at 426 cm^{-1}. Furthermore, every $[PS_4]^{3-}$ anion has only C_1 symmetry, and hence all degenerate modes of the above assuming T_d symmetry are expected to split depending on their degeneracy into two or three modes of symmetry *a*, that are IR and Raman active. The complete lifting of the degeneracy is confirmed predominantly for the ν_3 and ν_4 modes forming a distinct doublet of triplets as indicated in Figure 11. Remarkably, the split components of the ν_3 and ν_4 modes for **3** show a particularly alternating behavior as bands being intense in the IR spectrum are weak in the Raman spectrum and vice versa. Thus, for every of these modes, there is a sequence of strong-weak-strong absorptions in the IR spectrum and vice versa for the intensities of the Raman lines that gives strong evidence for our assignment.

The FT-Raman-spectra of **2**−**4** excited with λ_{exc} = 1064 nm are displayed in Figure 12. Besides the now merely detectable symmetrical P−S-vibrations ν_1 at about 430 cm^{-1} there are other very strong lines at about 100−250 cm^{-1} and 1950−2250 cm^{-1}. In agreement with the energy levels of Nd^{3+}[35−37] we attribute the lines with Raman shifts <250 cm^{-1} to transitions to Stark levels within the manifold of the electronic Nd^{3+} ground state $^4I_{9/2}$ and those with Raman shifts within the range 1950−2250 cm^{-1} to transitions from the electronic ground-state to the Stark levels of the first excited $^4I_{11/2}$ manifold. These transitions are especially well-resolved in the spectrum of **3** at 176 and 244 cm^{-1} for those of the $^4I_{9/2}$ manifold and at 1983, 2006, 2044, 2116, 2171, and 2217 cm^{-1} for the six levels of the $^4I_{11/2}$ manifold, probably because the crystal field in the $\{NdS_8\}$ polyhedron is less disordered and tighter (mean *d*(Nd−S) = 2.96 Å) than that in the closely related potassium salt **2** (mean *d*(Nd−S = 3.00 Å). As a consequence of the somewhat different crystal fields of the two crystallographically independent Nd^{3+} ions some of the electronic Raman (ER) lines are noticeably split and broadened in the FT-Raman spectrum of **4**. Because of the nephelauxetic effect[38] the baricenter of the $^4I_{11/2}$ manifold of Nd^{3+} in pure sulfur coordination in comparison to that in an oxo environment should be at slightly lower energy, but this cannot fully be confirmed considering the data of Xu et al.[37]

The ER effect has been shown to be a powerful tool to study low lying d-d or f-f transitions as these are allowed by group theoretical selection rules but are parity forbidden and hence weak in the absorption spectra. One of the most prominent examples among others is the ER spectra of the intraconfigurational transitions within the spin−orbit split ground state of low-spin Os^{4+} in $[OsBr_6]^{2-}$.[40] But even though ER spectroscopy has been studied for more than four decades now, it has nonetheless never realized the same as today's common use of absorption spectroscopy for mainly three reasons: First the experimentally accessible spectroscopic range in common Raman spectrometers is limited to about 8500 cm^{-1}; second the discrimination of ER from vibrational Raman transitions, as for instance in large molecules like porphyrins or phthalocyanines, is a challenge;[41] and last there is a great fortuity to find a selective resonance enhancement. Although the discrimination of the ER and vibrational Raman lines is currently of no doubt, our studies are experimentally limited to a range 100 < ν < 3000 cm^{-1} and therefore only transitions from the ground level to Stark levels of the ground-state and first excited-state are detectable. According to Albrecht's theory[42] the high intensity enhancement of up to 10^6 involving only totally symmetrical transitions by A-term scattering requires the close approach or coincidence of the excitation laser line with a strong dipole allowed electronic transition of the molecule. A much weaker enhancement is observed for the remaining transitions by B-term scattering when the excitation is between two interacting electronic states. Correspondingly, in the present study a resonant excitation with 1064 nm (~9400 cm^{-1}) via B-term scattering involving the $^4I_{13/2}$ (~6000 cm^{-1}) and $^4F_{3/2}$ (11240 cm^{-1}) intermediate states is supposed to be responsible for the significant enhancement by a factor of about 30 of the ER transition strength as compared to that of the totally symmetrical P−S stretching vibration ν_1.

(35) Jørgensen, C. K. *Orbitals in Atoms and Molecules*; Academic Press: London and New York, 1962.
(36) (a) Dieke, G. H. *Spectra and Energy Levels of Rare Earth Ions in Crystals*; Interscience: New York, 1968. (b) Schulz, H.; Reddmann, H.; Amberger, H.-D.; Kanellakopulos, B.; Apostolidis, C.; Rebizant, J.; Edelstein, N. M. *J. Organomet. Chem.* **2001**, *622*, 19–32.
(37) Xu, Y.-Z.; Wu, J.-G.; Sun, W.-X.; Tao, D.-L.; Yang, L.-M.; Song, Z.-F.; Weng, S.-F.; Xu, Z.-H.; Soloway, R. D.; Xu, D.-F.; Xu, G.-X. *Chem.—Eur. J.* **2002**, *8*, 5323–5331.
(38) Jørgensen, C. K.; Pappalardo, R.; Flahaut, J. *J. Chim. Phys.* **1967**, *62*, 444–448.
(39) Homborg, H. *Z. Anorg. Allg. Chem.* **1980**, *460*, 27–36. (b) Clark, R. J. H.; Stewart, B. *Struct. Bonding [Berlin]* **1979**, *36*, 1–80.
(40) Homborg, H. *Z. Anorg. Allg. Chem.* **1982**, *493*, 121–138.
(41) (a) Sievertsen, S.; Schlehhahn, H.; Homborg, H. *Z. Naturforsch.* **1994**, *49B*, 50–56. (b) Sievertsen, S.; Schlehhahn, H.; Homborg, H. *Z. Anorg. Allg. Chem.* **1993**, *619*, 1064–1072. (c) Galich, L.; Hückstädt, H.; Homborg, H. *J. Porphyrins Phthalocyanines* **1997**, *1*, 259–265. (d) Sievertsen, S.; Galich, L.; Homborg, H. *Z. Naturforsch.* **1995**, *50A*, 881–887.
(42) (a) Albrecht, A. C. *J. Chem. Phys.* **1961**, *34*, 1476–1484. (b) Albrecht, A. C.; Hutley, M. C. *J. Chem. Phys.* **1971**, *55*, 4438–4443.

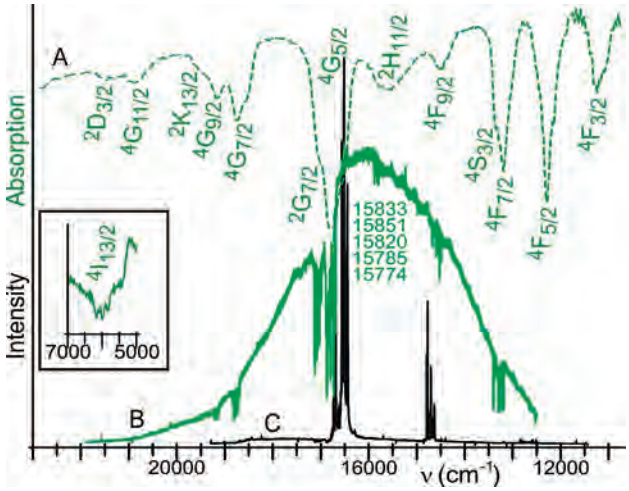

Figure 13. Comparison of the vis/NIR diffuse reflectance spectrum (A: hatched line; 293 K) and the emission spectra of **3** (B: LABS spectrum; λ_{exc} = 454.5 nm; ~15 K; C: luminescence spectrum; 514.5 nm; ~15 K).

The vis/NIR diffuse reflectance spectrum of **3** measured at 293 K (Figure 13A) displays a number of broad absorptions that are as well observed in the spectra of **2** and **4** and that are attributable to the well-known f-f transitions of the Nd^{3+} ion. Absorptions that will not be detailed in the following discussion are assigned as follows to electronic transitions from the $^4I_{9/2}$ ground state to excited states which are given in parentheses: 5830 ($^4I_{15/2}$), 11240 ($^4F_{3/2}$), 12290 ($^4F_{5/2}$), 13190 ($^4F_{7/2}$), 13340 ($^4S_{3/2}$), 14520 ($^4F_{9/2}$), 15600 ($^2H_{11/2}$), 16810 ($^4G_{5/2}$), 17010 ($^2G_{7/2}$), 18740 ($^4G_{7/2}$), 19160 ($^4G_{9/2}$), 19440 ($^2K_{13/2}$), 20900 ($^4G_{11/2}$), 21470 ($^2D_{3/2}$), 22930 cm^{-1} ($^2P_{1/2}$). The transition to $^4I_{13/2}$ expected to be at about 4000 cm^{-1} [35] has neither been detected in the diffuse reflectance spectra nor in the IR spectra. Optical band gaps were estimated from the very broad and intense absorption band extending far into the UV to be at about 3.50 eV for **2**, 3.15 eV for **3**, and 3.28 eV for **4**. These values are only lower limits because there are still some overlapping f-f transitions.

Figure 13B,C shows emission spectra obtained by excitation of **3** at ~15 K with the Ar^+ laser line at 454.5 nm (B) and 514.5 nm (C) together with the corresponding wavenumbers and assignments. Essentially comparable, but thoroughly more structured spectra have been observed for **2** and **4** that will not be discussed here. The emission spectrum (Figure 13B) excited at 454.5 nm just above the spin-forbidden $^2D_{3/2}$ manifold shows a very broad luminescence with half-bandwidth of ~4000 cm^{-1} covering almost completely the accessible spectral range of the Raman spectrometer and maximizing just between the $^4G_{5/2}$ and $^2H_{11/2}$ absorptions. The present study reveals no clear answer whether the origin of this luminescence is an intrinsic property of the Nd^{3+} ion or simply because of small impurities present in the sample. Nevertheless, although broad, the luminescence band is finely structured by a number of absorptions that without any doubt reproduce the corresponding Nd^{3+} absorptions as detailed in Figure 14A−D. Similar spectra, called according to the phenomenon "luminescence-absorption" or "LABS" spectra have been observed occasionally[40,42] when a broad intense luminescence is

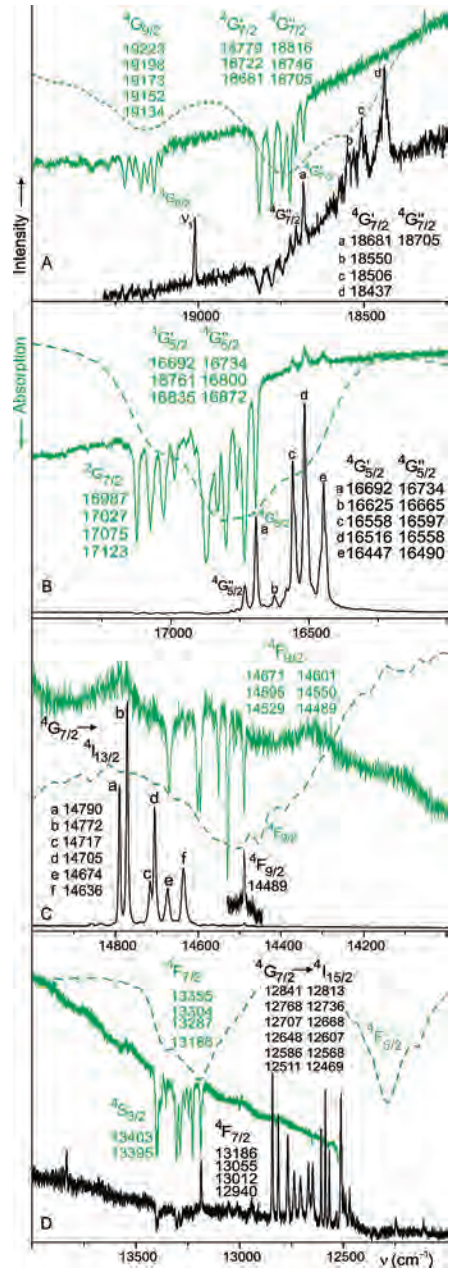

Figure 14. Details of the vis/NIR diffuse reflectance spectrum (hatched line; 293 K) and the emission spectra of **3** (LABS spectrum; λ_{exc} = 454.5 nm; ~15 K; luminescence spectrum; 514.5 nm; ~15 K). For clarity, the transitions involving the ground state $^4I_{9/2}$ are indicated only by the corresponding excited-state manifolds.

overlaying narrow weak electronic absorption bands predominantly of the d-d or f-f type, sometimes even permitting the detection of very weak absorptions that are otherwise hidden within the basis of strong charge-transfer bands.[39] As detailed in Figure 14A−D, the broad Nd^{3+} absorptions of the former diffuse reflectance spectrum have now changed into finely resolved narrow absorption lines forming multiplets according to their excited-state manifolds. In addition, as a consequence of the low temperature hot bands forming shoulders on the low energy wing of the absorption bands in the diffuse reflectance spectrum at 293 K are now missing, for example, for $^4G_{5/2}$ in Figure 13C or $^4G_{7/2}$ in Figure 14D.

The emission spectrum presented in Figure 13C and detailed and assigned in Figure 14A−D is obtained by

excitation with $\lambda_{exc} = 514.5$ nm on the high energy wing of the spin-allowed $^4G_{9/2}$ absorption (Figure 14A). The once broad emission has now turned into a number a very sharp and partly very intense luminescence lines. Four of them coincide with absorption lines at 18681 ($^4G_{7/2}$), 16692 ($^4G_{5/2}$), 14489 ($^4F_{9/2}$), and 13186 cm^{-1} ($^4F_{7/2}$) and are assigned to the lowest level of the corresponding spin-allowed manifolds. Transitions between $^{2S+1}L_J$ manifolds with $\Delta S = 0$, $\Delta L = \pm 2$ and $\Delta J = \pm 2$ are considered to be "hypersensitive". Accordingly, the hypersensitive $^4G_{5/2} \rightarrow {}^4I_{9/2}$ transition is split into two well separated components ($^4G'_{5/2}$ and $^4G''_{5/2}$; $\nu = 42$ cm^{-1}; Figure 14B), most likely because of marginally different Nd^{3+} ions being present in the crystal structure. A comparable but smaller splitting of 24 cm^{-1} is also observed for $^4G_{7/2}$ that is known to mix strongly with $^4G_{5/2}$[35,36] and is therefore to some extent hypersensitive as well. By far the most intense luminescence is that of $^4G_{5/2}$ followed by four very intense to medium luminescence lines a−e, that are attributed to the Stark levels of the ground manifold $^4I_{9/2}$. While d (176 cm^{-1}) and e (245 cm^{-1}) correspond to the ER lines in Figure 12, those at 67 (a) and 134 cm^{-1} (b) are supposed to be obscured in the ER spectrum for experimental reasons. The corresponding transitions of the split component $^4G''_{5/2}$ are very weak but nevertheless detectable as indicated (Figure 14B). The three most intense lines of these transitions are also observed for $^4G'_{7/2}$ (Figure 14A) and $^4F_{7/2}$ (Figure 14D), thus strongly confirming our assignment of the ER lines. There is still an intense luminescence multiplet starting at 14800 cm^{-1} (Figure 14C) and another one with much lower intensity (Figure 14A) that are tentatively assigned to the levels of the $^4G_{7/2} \rightarrow {}^4I_{13/2}$, $^4I_{15/2}$ transitions, respectively. Consequently, the $^4I_{13/2}$ manifold that has not been detected in the diffuse reflectance and IR spectra is found between 3891 and 4045 cm^{-1} in agreement with literature data,[35,36] and the $^4I_{11/2}$ manifold agrees well with our diffuse reflectance data between 5840 and 6212 cm^{-1}.

4. Conclusions

The successful synthesis of $K_9Nd[PS_4]_4$ (**1**), $K_3Nd[PS_4]_2$ (**2**), $Cs_3Nd[PS_4]_2$ (**3**), and $K_3Nd_3[PS_4]_4$ (**4**) is a further step in the direction of a promising chemistry of rare earth chalcogenophosphates with unusual structural features and spectroscopic properties. The structures of the title compounds with different motifs reflect the high flexibility of both the coordination of Ln^{3+} cations and the binding modes of $[PS_4]^{3-}$ anions. In the present cases, the Ln^{3+} ions show a clear preference for a bicapped trigonal prismatic or trigonal dodecahedral environment. In our ongoing investigations about rare earth chalcogen compounds a systematic variation of the ratios of the educt materials as well as of the heating conditions should lead to the formation of further new compounds, shedding light onto the relations between constituents of the compounds and structural and spectroscopic features.

Acknowledgment. The authors thank Ms. I. Jess and Dr. C. Näther for single crystal data collections, Ms. U. Cornelissen and Dr H. Homborg for measurements and helpful discussions about vibrational, absorption, luminescense and electronic Raman Spectra. Funding for this work was provided by the State of Schleswig-Holstein and the Fonds der Chemischen Industrie (FCI).

Supporting Information Available: X-ray crystallographic files (in CIF format) for compound **1**, **2**, **3**, and **4**. This information is available free of charge via the Internet at http://pubs.acs.org.

IC800143X